Remote Sensing of Environment 152 (2014) 333–344

Contents lists available at ScienceDirect

Remote Sensing of Environment

journal homepage: www.elsevier.com/locate/rse

Clear sky direct radiative effects of aerosols over Southeast Asia based on satellite observations and radiative transfer calculations

Nan Feng [a,*], Sundar A. Christopher [a,b]

[a] Department of Atmospheric Science, The University of Alabama in Huntsville, Huntsville, AL 35805, USA
[b] Earth System Science Centre, The University of Alabama in Huntsville, Huntsville, AL 35805, USA

ARTICLE INFO

Article history:
Received 8 January 2014
Received in revised form 9 July 2014
Accepted 12 July 2014
Available online 30 July 2014

Keywords:
Aerosol Radiative Effects
Southeast Asia
MODIS
CERES
Radiative transfer model

ABSTRACT

Using the Moderate Resolution Imaging Spectroradiometer (MODIS), Clouds and the Earth's Radiant Energy System (CERES) instrument, and a radiative transfer model (RTM), we provide a quantitative assessment of regional cloud-free diurnally averaged shortwave Aerosol Radiative Effects (AREs) at the top of atmosphere (TOA) and at the surface over Southeast Asia (SEAS, 10°S–20 N and 90°E–130°E). The spatial and temporal variations of the annual ARE are calculated based on satellite and ground-based measurements, supplemented by radiative transfer simulations. During 2001–2010, our results indicate that the *TOA* diurnally averaged ARE is -5.6 ± 0.8 Wm^{-2} over land and -4.8 ± 0.7 Wm^{-2} over ocean, respectively. In contrast, the *surface* ARE is -13.8 ± 3.2 Wm^{-2} based on radiative transfer calculations. For aerosol layers of 2 km in height with midvisible optical depth of 1.41 and single scattering albedo of 0.91, the shortwave radiative heating can exceed 0.8 K/day. Our results indicate significant inter-annual variability of aerosol radiative properties, which is extremely large over major emission outflow regions like SEAS. This study suggests that an integrated system of satellite data, model calculations coupled with ground-based and meteorological data sets is needed to assess Aerosol Radiative Effects on regional earth-atmosphere energy budgets.

1. Introduction

Although the impact of greenhouse gases on climate has been extensively studied, the role of aerosols also has measurable and equally significant impact on climate (Kaufman, Tanre, & Boucher, 2002). However, scientific understanding of the radiative effects due to atmospheric aerosols from regional to global scales is still uncertain, especially in regions with complex emission sources and land ecosystems such as Southeast Asia (SEAS) (IPCC, 2007; Reid et al., 2013). Previous studies have indicated that natural and anthropogenic aerosols alter the radiative energy budget by scattering and absorbing incoming solar radiation (the direct radiative effect) and also modify cloud properties (the indirect radiative effect) (Davison, Roberts, Arnold, & Colvile, 2004; Rajeev, Parameswaran, Nair, & Meenu, 2008). Depending on aerosol properties and the underlying surface albedo, the top of atmosphere shortwave aerosol direct radiative effects (ARE_{toa}) can be positive (warming effects) or negative (cooling effects). By absorbing incoming solar radiation, aerosols such as soot can both warm the atmosphere and cool the surface, whereas highly scattering type aerosols (e.g. sulfate) can cool the Earth's surface by reflecting more solar insolation and thereby increasing the planetary albedo (Eck, Holben, Slutsker, & Setzer, 1998; Satheesh & Ramanathan, 2000). Prior studies indicate that globally averaged ARE_{toa} values are negative but vary regionally depending on surface and aerosol characteristics (Yu et al., 2006). Large uncertainties are associated with current estimates of ARE_{toa}, that are largely due to the heterogeneous spatio-temporal distributions, magnitudes of aerosol loadings, uncertainties in characterizing microphysical and optical properties, and challenges in assessing their interactions with clouds.

Recently there has been a renewed emphasis on observational studies to provide better estimates of aerosol loading and ARE_{toa} that can be used for validating and constraining numerical models (Kahn, 2012). Observational estimates based on satellite and ground observations can provide reliable monitoring of aerosol emissions, transport, and its microphysical and optical properties, which can then provide realistic representations of regional aerosols in numerical models. Measurements of aerosol physical and chemical properties are also available from field campaigns conducted in major aerosol regimes over the world. These measurements can be used in radiative transfer models (RTMs) to estimate ARE_{toa} and surface radiative effect ARE_{sfc} (Christopher et al., 2000; Fu & Liou, 1993). However, only a very few direct measurements of atmospheric composition, aerosols, or cloud properties are available over SEAS. Satellite remote sensing can therefore serve as a useful tool to understand the impact of aerosols on climate (Reid et al., 2013).

Satellite data from the Moderate Resolution Imaging Spectroradiometer (MODIS) and Multiangle Imaging SpectroRadiometer (MISR) can provide routine global measurements of aerosol properties (e.g. aerosol optical

* Corresponding author.

http://dx.doi.org/10.1016/j.rse.2014.07.006
0034-4257/

depth). These observations can be used in conjunction with broadband data sets from Radiation Budget instruments such as Clouds and the Earth's Radiant Energy System (CERES) to estimate ARE_{toa} (Zhang, Christopher, Remer, & Kaufman, 2005a). Although previous studies have assessed ARE_{toa} over regions with high smoke aerosol concentrations such as Africa and South America (Sakaeda, Wood, & Rasch, 2011; Sena, Artaxo, & Correia, 2013), the spatial and temporal distributions of ARE_{toa} that are mainly caused by biomass burning smoke and industrial pollution over SEAS have not been studied in much detail. The ubiquitous cloud cover, sharp gradients in surface features, and complex aerosol characteristics increase the difficulties in conducting in-situ and remote sensing observations. By using observations from MODIS, CERES and AERONET along with calculations from the RTM, this study provides quantitative evaluation of regional cloud-free diurnally averaged ARE_{toa} and ARE_{sfc} over the entire SEAS region during a 10 year period from 2001 to 2010.

The major goals of this study are to:

a) Assess the ARE_{toa} in cloud free conditions using multi-year observations from MODIS and CERES instruments on board the Terra satellite;
b) Calculate ARE_{sfc} using satellite and AERONET data in radiative transfer calculations;
c) Compare these assessments with previous research;
d) Use aerosol vertical distribution to assess profile of radiative heating rates.

2. Data and area of study

2.1. Southeast Asian meteorology and aerosol particles

The study area includes the SEAS region between 10°S–20°N and 90°E–130°E which covers tropical to subtropical regimes (Fig. 1a, b

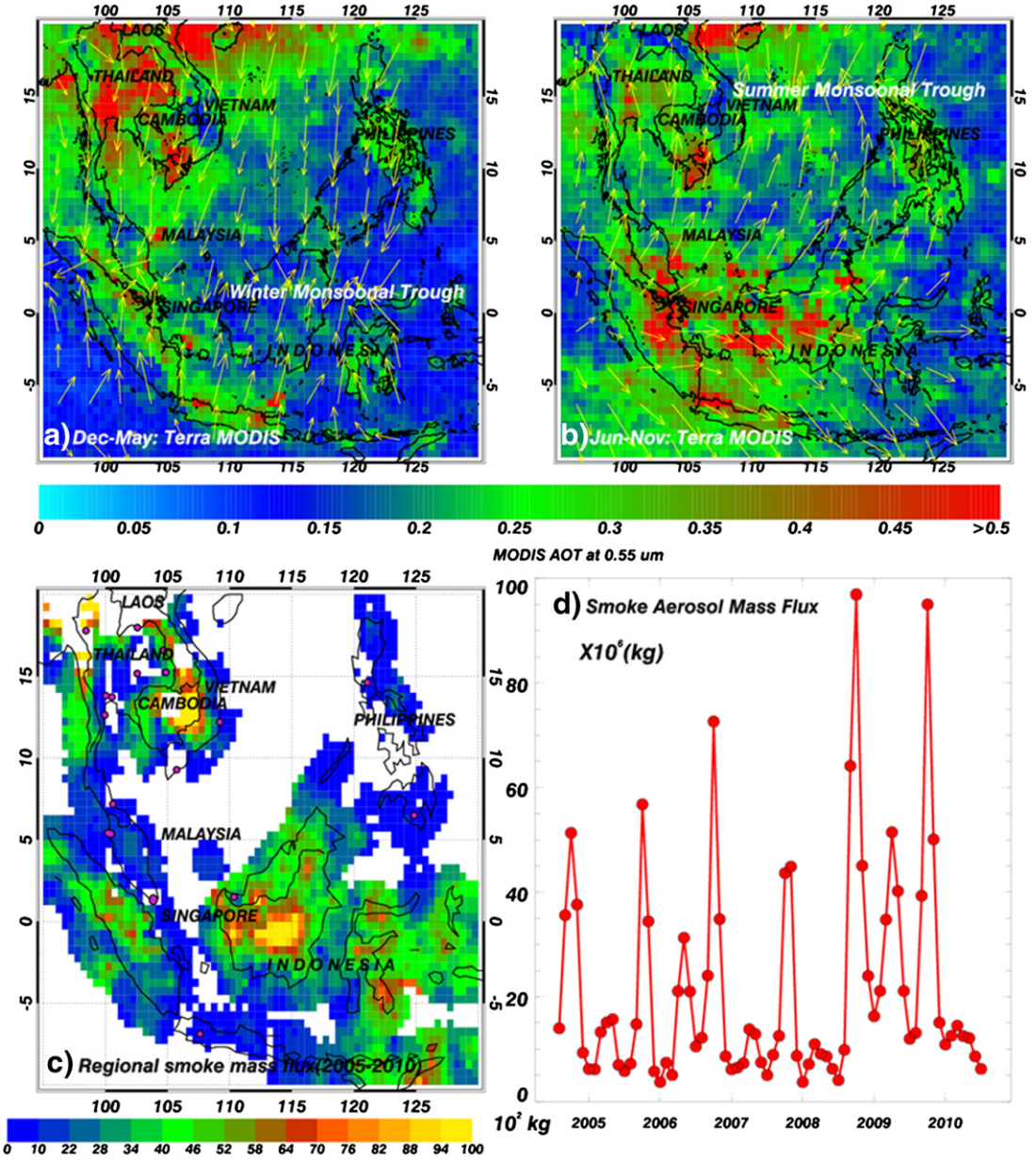

Fig. 1. Seasonal averaged aerosol optical depth (AOD) composites from MODIS collection 5.1 (550 nm) MOD04 products for each 0.5 × 0.5 degree grid point for (a) December to May and (b) June to November during the whole study period from 2001 to 2010. Also with NOGAPS winds at 850 hPa averaged over each period and plotted to show monsoonal characteristics (c) 0.5° × 0.5° spatial distributions of annual mean FLAMBE smoke aerosol mass fluxes, with ground-based AERONET sites (purple points). (d) The monthly variations of regional FLAMBE smoke aerosol mass fluxes ($\times 10^6$ kg) from 2005 to 2010.

and c). The climate of this region is mainly tropical which is hot and humid all year round with plentiful rainfall (monthly averaged value of 208.46 mm based on NASA's Tropical Rainfall Measuring Mission observations), but there is also a wet and dry season caused by seasonal shift in winds or monsoon. The rain forest in the region is the second largest on Earth. An exception to this type of climate and vegetation is the mountain areas in the northern region where high altitudes lead to milder temperatures and drier landscape. Previous studies have shown that aerosol particle loadings over SEAS can vary from a clean equatorial environment (i.e. clean air over islands in the Philippines and Indonesia), to high concentrations in individual smoke plumes (Reid et al., 2013). High concentrations of smoke aerosols can be generated from biomass burning which is also responsible for changing land cover in this region. According to the seasonal variations of midvisible aerosol optical depth (AOD) retrieved from Terra MODIS level 2 aerosol product during 2001–2010, high aerosol loadings can be seen from Thailand to Myanmar and appear thicker to the west in the North western part of the study area during the winter season from December to May (Fig. 1a). This is largely due to smoke aerosols from biomass burning activities combined with industrial and urban air pollution from farther west (Begum et al., 2006). During the winter season (Fig. 1a), the dry phase of the northeast monsoon is prevalent, which can transport biomass burning smoke aerosol further westward into the Indian Ocean (Lawrence & Lelieveld, 2010). In Fig. 1b, high AOD values are seen over megacities such as Singapore (1.28°N, 103.83°E) and Jakarta, Indonesia (6.2°S, 106.8°E) from June to November, which are correlated with anthropogenic and urban activities (See, Balasubramanian, & Wang, 2006; Zou & Hooper, 1997). In these metropolitan areas, there are significant emissions from automobiles and other anthropogenic activities related to the extremely high population density (Feng & Christopher, 2013). Under the effects of the strong southwest summer monsoon during this period, a fraction of insoluble pollutants, mostly from biomass burning, can still be transported towards the northeast, across the North Pacific basin, further reaching North America and beyond, which has also been highlighted by previous studies (Liang et al., 2007; Liu et al., 2003). The variations in aerosol speciation (e.g. agricultural burning, industrial and urban pollution, and sea salt) coupled with variability in land use, clouds, and precipitation, make the study area a unique ocean–atmosphere–land environment for a host of remote sensing and modeling systems (Reid et al., 2013).

2.2. FLAMBE emissions

The Fire Locating and Modelling of Burning Emissions (FLAMBE) (http://www.nrlmry.navy.mil/flambe/) data set derived from multiple satellites is in this study to specify the spatial and temporal distributions of smoke emissions (Fig. 1c and d). The emissions are calculated based on the total amount of fuel mass available for combustion, the average mass fraction of carbon in the fuel, the combustion factor, the fire averaged fine particulate matter emission factor over the burn period, the total area burned, and the average interval time (Reid et al., 2009). The FLAMBE dataset is representative of regional smoke emissions because of its use of appropriate land surface database and near real time information of satellite-based fire products (Wang et al., 2013). Two fire seasons among several SEAS countries can be identified by combining the spatial and monthly temporal distributions of regional FLAMBE smoke aerosol fluxes (Fig. 1c and d). The northern peaks during December to May are much more intense than the southern peaks during June–November (Reid et al., 2013).

2.3. Satellite and ground observations

The satellite and ground measurements used in this study include data from MODIS, MISR, AERONET, and CERES.

The MODIS on board the NASA's Earth Observing System (EOS) constellation of satellites has 36 channels that range 0.4 to 14 μm, that provides global values of AOD and other parameters (Levy, Remer, Mattoo, Vermote, & Kaufman, 2007). The MODIS collection 5 AOD used in this study has an estimated uncertainty of $0.03 \pm 0.05\tau$ over ocean and $0.05 \pm 0.15\tau$ over land (Levy et al., 2007; Remer et al., 2005). The MODIS land albedo product (MCD43C3) (Schaaf et al., 2002) is a 16 day composite in 0.05° latitude/longitude spatial resolution that is used as input for the RTM calculations.

The MISR on board Terra has 9 cameras that measures reflected solar radiance in four spectral bands (centered at 446, 558, 672, 866 nm) at nine view angles in the forward and afterward directions along the flight path (nadir, ±70.5°, ±60°, ±45.6°, ±26.1° from nadir). The wide range of view angles makes it feasible to evaluate surface contribution to the TOA radiance accurately and retrieve aerosol properties both over ocean and land surfaces including bright desert regions (Diner et al., 1998; Kahn et al., 2005). MISR datasets are also used to assess single scattering albedo (SSA) over the area. Even though the MISR SSA is considered Beta Quality for quantitative use, it provides useful information, especially in areas where there is no AERONET data.

The AERONET is a federation of about 200 ground based measurement sites around the world (Holben et al., 2001) and provides spectral measurements of sun and sky radiance for cloud free conditions (Smirnov, Holben, Eck, Dubovik, & Slutsker, 2000). Cloud-free AOD and inversion based retrievals of SSA, asymmetry parameter (g) and fine mode fraction (FMF) from AERONET level 2.0 aerosol products are used in this study for validating satellite derived aerosol optical properties over selected regions. We will further use these properties in a delta four stream RTM (Fu & Liou, 1993) to estimate ARE_{toa} and ARE_{sfc}.

The CERES is a broadband instrument on board both Terra and Aqua satellites (Loeb & Kato, 2002). It measures solar and terrestrial radiances in three broadband channels (shortwave (0.3–5 μm), window (8–12 μm), and total (0.3 > 100 μm)) at a spatial resolution of 20 km at nadir. In this study, we used the CERES Single Scanner Footprint (SSF) product which contains instantaneous pixel level data for a single scanner that is collocated with the high-resolution MODIS imager (CER_SSF_Terra-FM1-MODIS_Edition 3A). In this product, the higher-resolution MODIS data such as AOD (10 km × 10 km), scene identification, and cloud and aerosol properties are averaged over the larger CERES footprint using point spread functions (Smith, 1994). Shortwave fluxes from the regions containing aerosols (identified by MODIS) and from both cloud free (from MODIS) and aerosol free regions (i.e. clear sky fluxes) will be used from the SSF product (Section 3.1 and Fig. 2a).

3. Methodology

3.1. Clear sky Aerosol Radiative Effects from the satellite observations

Although SEAS is dominated by ubiquitous clouds during all seasons (monthly averaged cloud cover fraction is >60%), aerosol particles can still play a primary role on the regional energy budget under clear sky conditions, which is the focus of this study. The difference in TOA fluxes between the CERES clear and aerosol pixels is called the direct ARE_{toa}, which provides a quantitative assessment of how aerosols change the TOA shortwave fluxes (Christopher, Zhang, Kaufman, & Remer, 2006). The clear sky flux (F_{clr}) and aerosol sky flux (F_{aero}) cannot be obtained for the same pixel during the same satellite overpass time. Therefore, approximations are needed to calculate F_{clr}. Previous studies have used the lowest shortwave flux over a 10–15 day time period to obtain F_{clr}, while others have used RTM calculations to report F_{clr} under zero AOD conditions (Christopher & Zhang, 2002a; Procopio et al., 2004). Our measurement-based methods in Fig. 2a show that the F_{clr} can be estimated by using linear regressions between MODIS AOD and CERES shortwave fluxes. The regression line representing the relationship between shortwave fluxes and AOD is based on pixel-level data for each 0.5° × 0.5° latitude/longitude grid as a function of months, wind speeds (3 m/s bins), and solar zenith angle (θ_0, 6° bins). Clear-sky data are used

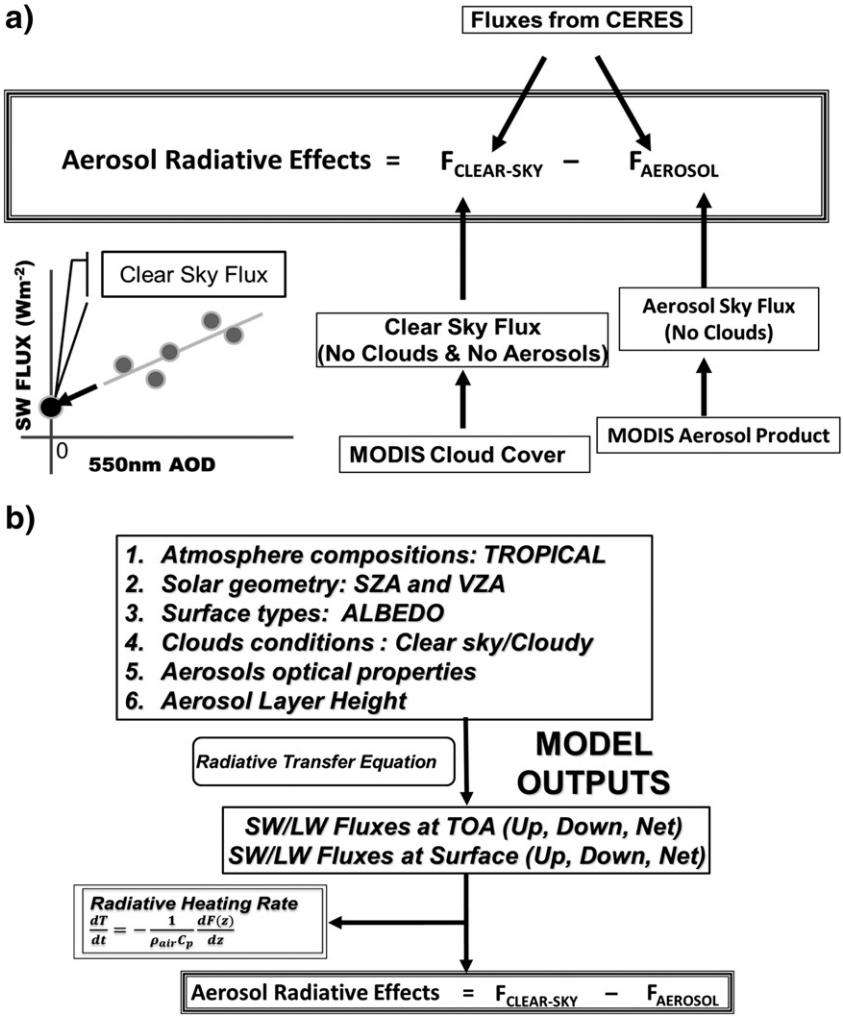

Fig. 2. a) The flowchart description of SW ARE estimations based on satellite observations. b) The flowchart description of SW ARE estimations and radiative heating rate calculations based on delta four stream RTM.

where clear area percent coverage is above 99% in each CERES foot print. Besides, sample biases due to different spatial resolutions between MODIS (10×10 km^2) and CERES footprint (20×20 km^2) are estimated to globally reduce ARE_{toa} by an average of 30% (Christopher & Jones, 2008). To mitigate this bias we have multiplied mean MODIS AOD minus the CERES AOD by a radiative efficiency value (Wm^{-2}/AOD) to correct the clear sky sample biases. The flux extrapolated to zero AOD is then identified as the F_{clr} (Christopher, 2011). More details are described by previous studies (Christopher, 2011; Patadia, Gupta, Christopher, & Reid, 2008; Zhang, Christopher, Remer, & Kaufman, 2005b). The slope estimated from the regression indicates that the relationship between ARE_{toa} and AODs may be affected by outliers. To minimize these effects, median values are used to develop regressions. Since biomass burning aerosols in SEAS are largely dominated by fine mode particles, their impact in the longwave is negligible (Kaufman, Karnieli, & Tanre, 2000). Hence, the shortwave instantaneous ARE_{toa} is first calculated, which was further converted to diurnally averaged values based on the variations of solar zenith angles (θ_0) and aerosol optical properties during a day (Remer & Kaufman, 2006; Zhang et al., 2005a). To accomplish this, a look-up-table for the scaling factor between diurnal averaged ARE_{toa} and the instantaneous values obtained during the Terra overpass time are calculated based on radiative transfer model calculations by using different aerosol models and θ_0 values computed from every hour, every month, and every 5° latitude belts over the domain. Previous studies have shown that uncertainties of the scaling factor in this conversion process are ± 0.1 (Zhang et al., 2005a). The methodology is outlined in Fig. 2a.

3.2. Aerosol Radiative Effects from the radiative transfer model

A four stream radiative transfer model has been applied in this study, which is a delta-four stream plane-parallel broadband radiative transfer model to calculate the flux at the TOA and at the surface in both clear and cloudy conditions (Charlock & Alberta, 1996; Fu & Liou, 1993). It was then modified for calculation of radiative effect of aerosols, such as smoke (Christopher & Zhang, 2002b; Christopher et al., 2000; Wang et al., 2003) and dust (Christopher, Wang, Ji, & Tsay, 2003; Liao & Seinfeld, 1998; Wang et al., 2003). The gas absorption, water vapor absorption, and Rayleigh scattering are included in the model calculations. The model divides the shortwave spectrum (0.2–4 μm) into 6 bands 0.2–0.7, 0.7–1.3, 1.3–1.9, 1.9–2.5, 2.5–3.5, and 3.5–4.0 μm and further divides the first band (0.2–0.7 μm) into 10 sub-bands. For the principal atmospheric gases, the difference between the four-stream and line-by-line irradiance calculations is within 0.05% (Fu & Liou, 1993). Overall, for the computations of solar irradiance covering the entire shortwave spectrum, the calculated values are within 5%, when compared to adding–doubling calculations (Liou, Fu, & Ackerman, 1988). As seen in Fig. 2b, to complete the calculations based on radiative transfer equations, the delta-four stream RTM requires inputs including atmosphere compositions (e.g. the vertical profiles for the water vapor, ozone),

solar geometry information (e.g. solar zenith angle and view zenith angle), surface information (e.g. wavelength dependent surface albedo), cloud conditions (i.e. clear sky or cloud type, cloud layer heights), and aerosol optical properties and layer height (e.g. SSA, g, and AOD). The model then calculates the shortwave fluxes at different layers from the surface to the TOA. The difference between the net fluxes over clear and aerosol sky regions is defined as the Aerosol Radiative Effect at the specific layer (e.g. surface or TOA). Then the vertical profiles of radiative heating rate due to aerosols can be further calculated according to the net fluxes for different layer heights (Fig. 2b). The original version of the radiative transfer code includes aerosol properties (e.g., SSA, g and extinction coefficient) of 18 different aerosol types (e.g., D'Almeida, Koepke, & Shettle, 1991; Tegen, 2003; Tegen & Lacis, 1996). To increase the accuracy of calculations, we added aerosol property information mainly derived from ground-based observations (e.g. AERONET). Aerosol properties (e.g. spectrally dependent SSA) over the area without ground-based observations are provided by the Terra MISR level 2 aerosol product. The surface albedo over land is supplied by 0.05° × 0.05° MODIS global albedo product (MCD43C), while the albedo for ocean surface has been assumed to be default values from the RTM. Aggregate MODIS albedos, MISR and AERONET SSAs are aggregated to a common and consistent 5° × 5° grid to be consistent with the RTM calculations over the domain. For each month, radiative transfer calculations have been performed over the ocean and land for each 5° × 5° grid as a function of θ_0, wavelength dependent surface albedo and aerosol properties, along with the default tropical atmospheric profiles (McClatchey, Fenn, Selby, Volz, & Garing, 1971) of water vapor, temperature, and other atmospheric constituents (e.g., O_3).

4. Results and discussions

In this section, ARE_{toa} was first calculated from MODIS and CERES data sets. In Section 4.2, we investigate the clear sky Aerosol Radiative Effects at both TOA and surface according to radiative transfer model calculations. Then, in Section 4.3 our results are compared with previous research. Finally, the vertical profiles of aerosol radiative heating rate during the period where biomass burning events are prevalent have been estimated.

4.1. Aerosols direct radiative effects based on satellite observations

Multiple sensors on board satellites have been used for studying aerosol climatic impacts from an observational perspective (Christopher & Jones, 2008; Feng & Christopher, 2013; Patadia, Christopher, & Zhang, 2011; Patadia et al., 2008). In Fig. 3, by using box and whisker plots while overlaying the density map of data, we describe the linear relationships and ranges of the MODIS AOD values and the measurement-based estimations of ARE_{toa}. Along with the increase of AOD values, stronger ARE_{toa} values (more negative) are observed over both land and ocean, which represent major cooling effects caused by stronger aerosol loadings over the SEAS region. The box and whisker plots in Fig. 3a and b are used to indicate the 25th, median, and 75th percentile of data for each 0.2 AOD bin. Due to different aerosol properties and heterogeneous surface albedos, larger variations of ARE_{toa} in each AOD bin can be clearly seen over land than over ocean areas, especially when the AOD values are lower than 0.5. The pixel level ARE_{toa} values for each month and each grid are computed based on the difference between TOA shortwave flux over clear sky and aerosol skies as a function of wind speed, solar zenith angle, and surface types. Fig. 4a shows the spatial distributions of the diurnally-averaged ARE_{toa}, which are calculated over land and ocean independently, but are combined, in the same figure for comparison purposes. Previous studies have shown that ARE_{toa} values vary as a function of regions (Feng & Christopher, 2013; Patadia et al., 2008; Yu et al., 2006). The regional patterns of ARE_{toa} compare well with the distributions of aerosol loadings over the regions with large AODs close to the coastal regions of Thailand, Vietnam, and South-eastern China that are from a combination of biomass burning smoke and industrial pollution (Kaufman et al., 2002). Over land, higher ARE_{toa} values are largely due to anthropogenic pollution over megacities, e.g. Jakarta and Singapore (See et al., 2006; Zou & Hooper, 1997). In contrast, large AOD values in Southern China, Thailand, and Eastern Indonesia do not result in strong ARE_{toa} values. This is due to the combined effects of aerosol and surface properties from diverse ecosystems (Patadia et al., 2008). For more absorbing aerosols, the overall ARE_{toa} can change from a negative to a positive value based on aerosol properties and the underlying surface. However, annual averages over 1° × 1° grids in Fig. 4 are largely negative. This can also been seen in Fig. 4b, which shows both yearly and monthly variations of diurnally averaged ARE_{toa} from 2001 to 2010. The highest regionally-

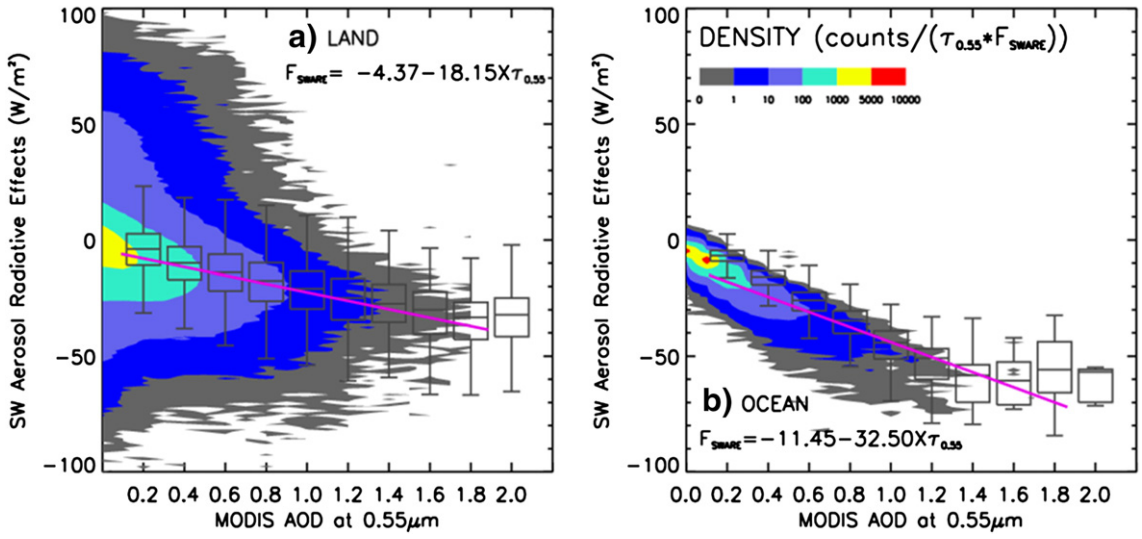

Fig. 3. Shortwave Aerosol Radiative Effect (SW ARE) as a function of MODIS AOD at 0.55 μm for the region of interest during the period of 2001 and 2010 over a) land and b) ocean, respectively. The colors of polygons represent different densities of data points, while the density is calculated based on the number of collocated points in the area of 0.1 $\tau_{0.55}$ and 1 Wm^{-2} SW ARE. The red solid lines represent the slopes of linear regression between median values of SW ARE and AOD for each 0.2 AOD bin, while linear equations are also shown in the inset.

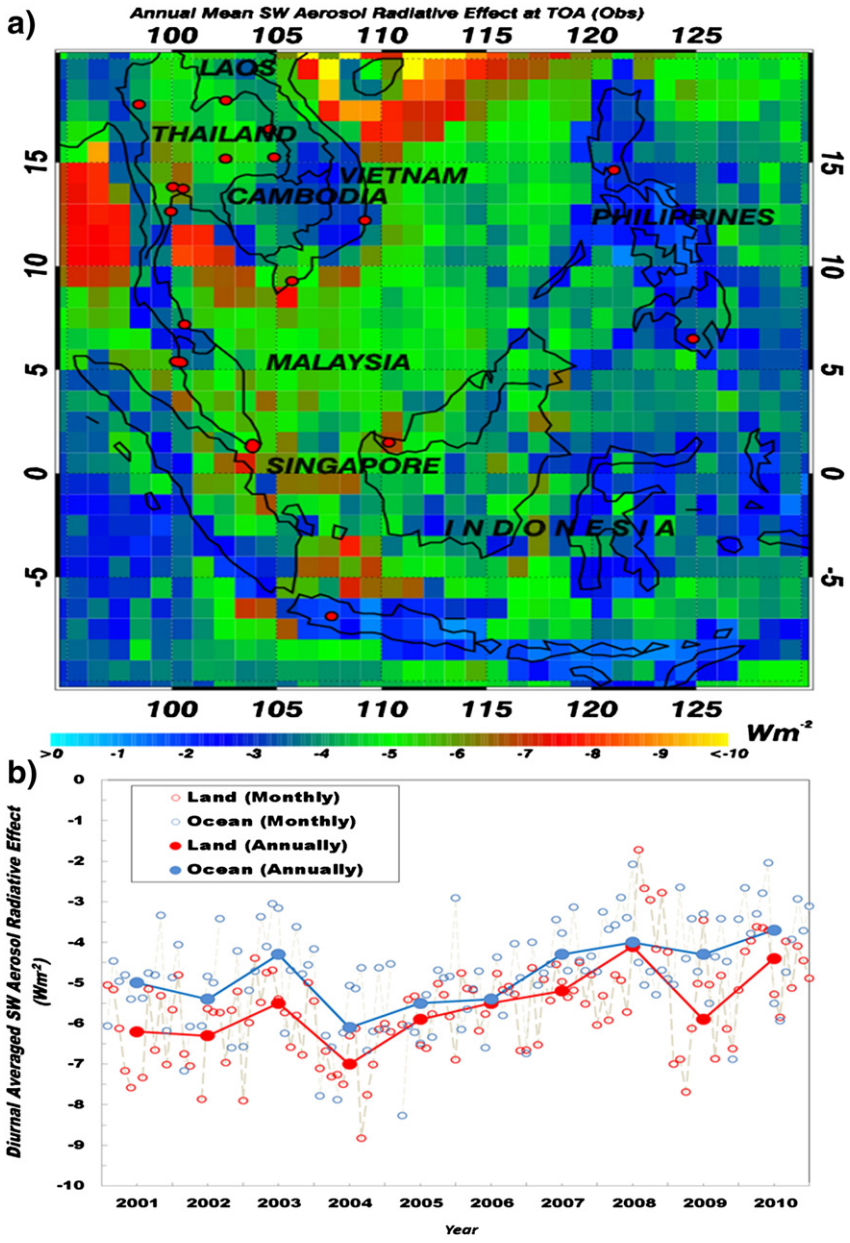

Fig. 4. a) Regional pattern of annual mean SW ARE at the top of atmosphere from satellite observations (2001–2010), where negative values indicate shortwave cooling due to aerosols. SW ARE over land and ocean is calculated respectively, but combined in the same figure. b) Decadal variations of regional mean SW ARE during 2001 and 2010 (filled big circle points), along with the monthly variations of AREs as backgrounds (unfilled small circle points).

averaged ARE_{toa} values are during 2004 with values of $-7.03\ Wm^{-2}$ and $-6.14\ Wm^{-2}$ over land and ocean, respectively. The lowest values are $-4.20\ Wm^{-2}$ over land in 2008 and $-3.67\ Wm^{-2}$ over ocean in 2010. Generally, the ARE_{toa} over both ocean and land shows similar variation with time except for some slight shifts in their monthly variations possibly indicating the transports of aerosols between land and ocean due to seasonal monsoons.

The peak (valleys) ARE_{toa} values with less (more) negative values indicate more (less) absorptive aerosols that are ubiquitous over the area when compared to other months. Although the peaks and valleys of monthly averaged ARE_{toa} values are not completely matched with the FLAMBE smoke emission data in Fig. 1d, two peak values due to two fire seasons among SEAS countries can still be identified for each year. The decreasing trends of ARE_{toa} (closer to zero) from 2005 to 2010 are matched with the increasing trends of FLAMBE smoke emissions for the same period in Fig. 1d. The slight mismatch of monthly variations between two data sets also indicates that rather than smoke aerosols, some other types of aerosols in this region such as dust, urban haze, or industrial pollutants can effectively contribute to the total ARE_{toa} values. Moreover, land cover changes due to deforestation and inter-annual

Table 1
TOA shortwave Aerosol Radiative Effects over Southeast Asia (10°S–20°N and 90°E–130°E) from satellite observations. All data are based on the mean ± standard deviations of annual averaged results during the period of 2001 to 2010.

	Land	Ocean
Clear-sky total AOD	0.24 ± 0.04	0.17 ± 0.03
Shortwave clear sky flux	150.0 ± 8.6 Wm^{-2}	76.9 ± 5.6 Wm^{-2}
Shortwave aerosol sky flux	160.9 ± 2.6 Wm^{-2}	87.7 ± 1.6 Wm^{-2}
Instantaneous SW ARE	−12.8 ± 2.1 Wm^{-2}	−10.5 ± 1.5 Wm^{-2}
Instantaneous SW efficiency	−32.9 ± 9.6 $Wm^{-2}\ \tau^{-1}$	−62.7 ± 2.5 $Wm^{-2}\ \tau^{-1}$
Diurnal SW ARE	−5.6 ± 0.8 Wm^{-2}	−4.8 ± 0.7 Wm^{-2}
Diurnal shortwave efficiency	−20.6 ± 2.4 $Wm^{-2}\ \tau^{-1}$	−28.5 ± 1.0 $Wm^{-2}\ \tau^{-1}$

climate variability (e.g. the El Niño/Southern Oscillation, ENSO) can also impact the yearly variations of aerosol systems and their climatic impacts over this region (Reid et al., 2013).

The annual mean ARE_{toa} information from measurement-based estimations is further given in Table 1. The mean and standard deviations are computed based on the yearly averaged results during the 10 year period from 2001 to 2010. Annually averaged shortwave fluxes of clear and aerosol skies over land area are both much higher than that over ocean, whereas their differences are used to calculate instantaneous aerosol direct radiative effects. The diurnally averaged annual ARE_{toa} in the whole region ranges from -14.15 to 2.40 Wm^{-2} with mean values of -5.6 Wm^{-2} over land area and -4.8 Wm^{-2} over ocean corresponding to a mean clear-sky total AOD (from CERES footprint data) of 0.24 ± 0.04 and 0.17 ± 0.03, respectively. A detailed comparison between our results with previous work can be seen in Section 4.3. Furthermore, shortwave radiative efficiency (Wm^{-2} per unit AOD) representing the efficiency of aerosols in perturbing the shortwave radiation at the top of atmosphere is also shown in Table 1, which is widely known as a key parameter for studying the climatic effects of aerosols. Zhang et al. (2005b) reported that the aerosol radiative efficiency is sensitive to the FMF where higher fine mode fraction values can result in lower aerosol efficiency. Fine mode fraction is the ratio of fine mode aerosols to total aerosols and is higher for regions where submicron aerosols (e.g. biomass burning) dominate. Therefore, using FMF to separate aerosols by size provides some information as to which aerosols might be anthropogenic in origin (smaller particles, e.g. biomass burning smokes) and which might be from natural, wind-generated sources (larger particles, e.g. sea salt). In this study, the *instantaneous* shortwave aerosol efficiencies are -32.9 ± 9.6 Wm^{-2} τ^{-1} over land and -62.7 ± 2.5 Wm^{-2} τ^{-1} over ocean that are both within the range reported by previous regional studies (Christopher, Gupta, Haywood, & Greed, 2008; Patadia et al., 2008). It can be seen that *diurnal averaged* shortwave efficiencies of aerosols over land are about -20.9 Wm^{-2} τ^{-1} that is less negative when compared with aerosol radiative efficiency values over ocean areas. This is because the aerosols over land, mainly from biomass burning and anthropogenic pollutions, have higher absorptivity than those over ocean, i.e. sea salt aerosol (Doherty et al., 2005; See et al., 2006). Also higher and more variable surface albedos over land can also decrease the aerosol radiative efficiency. Based on results for our current study, we can conclude that aerosol effects at the TOA are negative thereby cooling the surface. However, to obtain the surface radiative effects, ground-based measurements or radiative models are necessary.

4.2. Aerosols direct radiative effects based on radiative transfer model calculations

Numerical modeling simulations have reported a clear sky *diurnally averaged* ARE_{toa} of -25 Wm^{-2} over land surfaces which is mainly attributable to sulfate, black carbon, and organic carbon (Collins et al., 2002). Larger ARE_{sfc} can be expected in regions that have a large ARE_{toa} value but it depends on surface conditions, aerosol properties (e.g. optical depth). A sensitivity analysis conducted by Wang et al. (2013) over Northwest China has shown that both ARE_{toa} and ARE_{sfc} estimates based on RTM calculations are largely controlled by surface albedo, SSA, and AOD. For this section, the properties (e.g. SSA, g, AOD) of atmospheric aerosols over both land and ocean are collected from nearest ground AERONET sites or MISR level 2 aerosol products, which are used to construct the relationships between simulated AOD and ARE. The AOD at 0.55 μm ($\tau_{0.55}$) is then collected from Terra MODIS observations to calculate ARE_{toa} and ARE_{sfc}. In Fig. 5a, highly-absorbing aerosols with lower SSA (ω_0 at 0.55 μm <0.90) can be seen in the north-western area over SEAS due to large amounts of biomass burning smoke aerosols. Fig. 5b indicates that higher land surface albedo ($\alpha > 0.15$) can be observed by MODIS over maritime continents (e.g. Indonesia, Malaysia, and Brunei) due to frequent fire activities that convert peat swamp forest into bare land (Reid et al., 2013). This land use change process, along with the differences in aerosol properties, makes the ARE at both the TOA and the surface to be weaker in the maritime continents than those in the Indo-China region areas of peninsular SEAS based on our RTM calculations (Fig. 5c and d). RTM-derived ARE_{toa} in Fig. 5c is different with results from the CERES-derived (Fig. 4) in magnitudes and distributions, because model calculations are highly determined by the parameterizations of surface conditions and aerosol properties (e.g. ω_0, g and AOD). Annual mean ARE_{toa} estimates from satellite measurements can be compared with the results from RT calculations by adjusting both results into $5^\circ \times 5^\circ$ grid. The underestimations in the southern region ($<5^\circ$ N) with few ground-based observations can be found among those comparisons, which is due to frequent high values of SSA inputs retrieved from MISR in the northern region ($>5^\circ$ N). Lowering the SSA to around 0.85 in idealized condition provides better correlations between model and observations indicating the need for more reliable SSA data. Additionally, when compared to the maritime continents in the southern region of SEAS, the diurnally averaged ARE_{toa} values from RTM calculations over Indo-China region are better correlated with satellite measurements due to more data availability from ground-based observations. Very few AERONET sites are available in the maritime continental regions in countries like Malaysia and Indonesia thereby making it difficult to characterize aerosols optical properties in our calculations. The lack of adequate observations also results in more latitudinal variations of ARE values in the northern portions of the study regions when compared to the southern part of SEAS. The total clear sky annual mean diurnally averaged ARE_{toa} is -4.2 ± 1.2 Wm^{-2} and ARE_{sfc} is -13.8 ± 3.2 Wm^{-2} (mean ± standard deviations over the region), although both results are calculated separately over ocean and land surface. By absorbing or scattering the incoming solar radiation, the atmospheric aerosol particles over SEAS showed direct cooling/negative effects at both TOA and surface while the difference between ARE_{toa} and ARE_{sfc} implies warming/positive effects (7.6 ± 2.5 Wm^{-2}) in the whole atmospheric column. Based on retrieved SeaWiFS product, Chou, Chan, and Wang (2002) derived the surface to TOA ARE ratio of 2.5 in Southeast Asia due to the 1997 Indonesian fires. This ratio is reported to be too small since the aerosol absorption over ocean is underestimated by assuming a uniform spectrally independent SSA for both dust and smoke aerosols ($\tau_{0.55} > 0.3$). Podgorny et al. (2003) reported a ratio of 3.3 between ARE at surface and TOA, which is much closer to this study. Diurnally-averaged shortwave aerosol radiative efficiency calculated by the RTM is in the range of -10.9 to -20.0 $Wm^{-2}/\tau_{0.55}$ at TOA and -38.6 to -59.8 $Wm^{-2}/\tau_{0.55}$ at the surface while more absorptive aerosols (e.g. biomass burning smoke) with lower SSA can produce larger radiative efficiency (more negative) at both TOA and surface (e.g. Srivastava, Ramachandran, Rajesh, & Kedia, 2011). The diurnally averaged ARE_{sfc} is -16.2 Wm^{-2} from Dec to May and -10.4 Wm^{-2} from Jun to Nov for SSA values of 0.90 ± 0.04 and 0.94 ± 0.04, respectively. The stronger ARE with lower averaged SSA in the winter monsoon period could be due to more intense biomass burning activities in the northern area of SEAS during December to May with higher emissions of smoke aerosols over both ocean and land area every year.

4.3. Comparison with previous studies

In this section we compare our results with previous studies (Table 2). Such comparisons are challenging because the selected areas of study and the algorithms used to make these estimations are usually different among studies. For example, Yu et al. (2006) used MISR AOD along with assumed aerosol properties in radiative transfer models and report Aerosol Radiative Effects in different regions where the ARE_{toa} over SEAS (0°N–30°N and 90°E–180°E) is about -6.0 Wm^{-2} over land with a mean AOD value of 0.31 and -4.6 Wm^{-2} over ocean with a mean

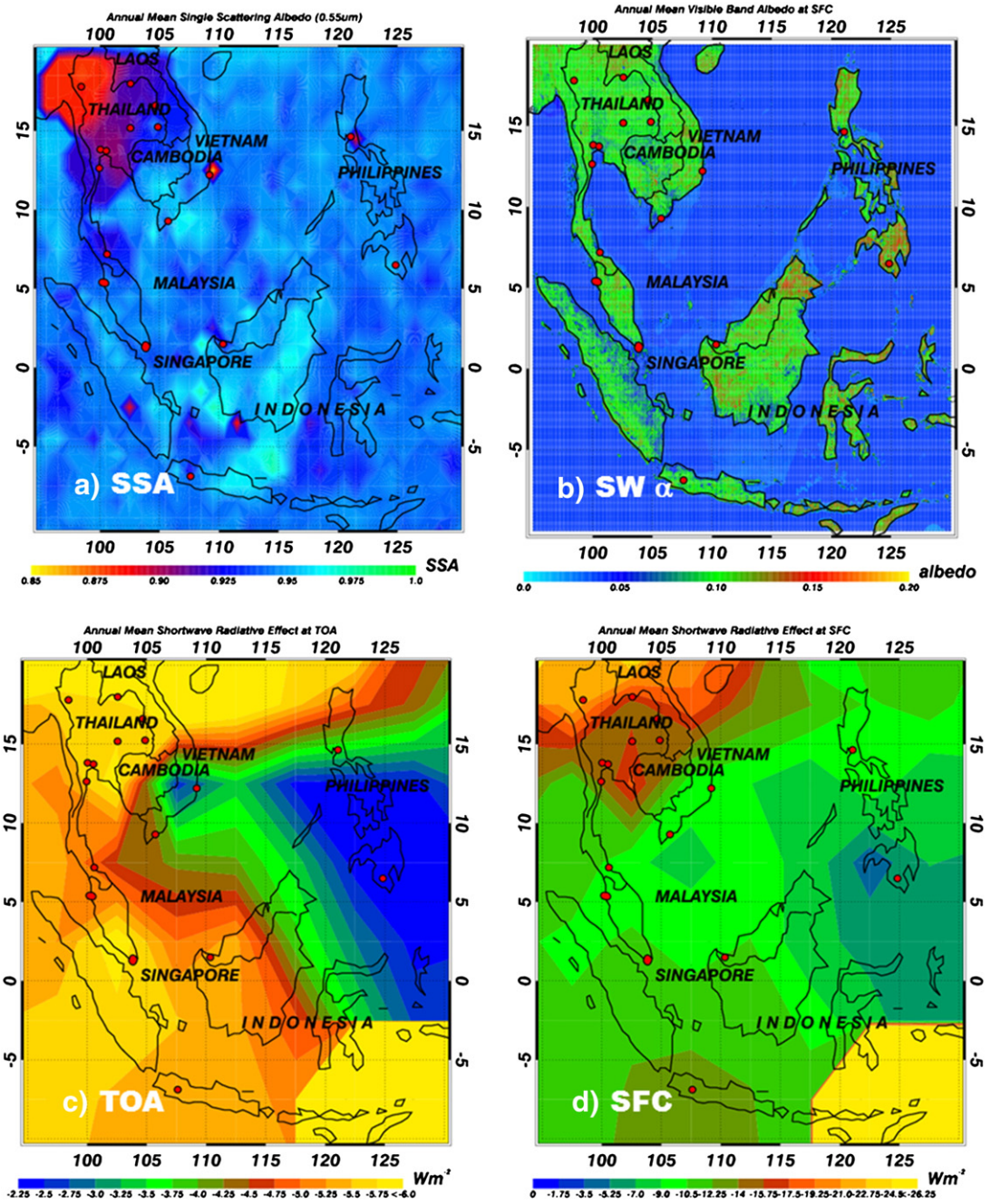

Fig. 5. Spatial distributions of annual mean (a) single scattering albedo (0.55 μm) from the ground-based AERONET aerosol inversion product and MISR level 2 aerosol products and (b) surface albedo at visible band (0.55 μm) from MODIS albedo product (MCD43C3), while albedo for ocean surface has been assumed to be defaulted values in the RTM. Regional contour maps of TOA (c) and surface (d) diurnally averaged SW ARE based on delta four stream RTM calculations. SW ARE over land and ocean is calculated respectively, but combined in the same figure. (Aerosol optical properties are from nearest AERONET observations, SW ARE for each day is computed from TERRA MODIS retrieved AOD at 0.55 μm based on the linear relationships between AOD and SW ARE from RTM calculations for each 5° × 5° grid).

AOD value of 0.13 (Table 2). The difference between satellite-model integrated estimation in Yu et al., 2006 and our study is due to heterogeneous aerosol loadings and the difference in study regions. Overall differences are likely due to the use of different datasets and cloud screening techniques as well. Yu et al. (2006) used level 3 MISR, 1° × 1° AOD values for land and MODIS level 3, 1° × 1° AOD values for ocean while we use level 2 MODIS AOD collocated in CERES SSF products. Also, we use stringent cloud screening criteria to ensure that the CERES data are not contaminated with clouds while requiring 99% of the CERES footprint to be cloud free. However, from Table 2, we still can see that the diurnally averaged ARE_{toa} from different studies generally ranges from −1.6 to −7.6 Wm^{-2} (AOD ranges from 0.12 to 0.25). To better compare the studies with different regional AOD values, the radiative efficiency is used to make this comparison. This is also the linear regression slope between ARE_{toa} and AOD. From Table 2, we find that the efficiency from various studies has a range from −20 to −45 $Wm^{-2}\,\tau^{-1}$ with a mean of -27 ± 10 $Wm^{-2}\,\tau^{-1}$. From 10 years (2001–2010) of analysis, the aerosol radiative efficiency in our study is −24.5 and 49.2 $Wm^{-2}\,\tau^{-1}$ at the TOA and surface respectively. Sena et al. (2013) used CERES/MODIS retrievals along with AERONET observations and discrete-ordinate radiative transfer (DISORT) model to study shortwave radiative effects due to biomass burning smoke aerosols at both TOA and surface over Amazon forests from 2000 to 2009 during the biomass burning seasons (August and September) and reported the diurnally averaged shortwave aerosol

Table 2
Top of atmosphere and surface cloud-free shortwave biomass burning smoke aerosol radiative forcing from combined narrowband and broadband satellite observations and radiative transfer calculations.

Reference	Area of study	Data used/time period/field experiment	AOD and reported wavelength at 0.55 μm	Top of atmosphere		Surface	Averaging method
				SWARF (Wm^{-2})	Forcing efficiency ($Wm^{-2}\,\tau^{-1}$)	SWARF (Wm^{-2})	
Sena et al. (2013)	Amazon	Terra-MODIS/CERES/DISORT code, Aug–Sep, 2000–2009	0.25	−5.6	$-13.1/\tau_{0.55}$	N/A	24 h Mean
Patadia et al. (2008)	Amazon	Terra-MISR/CERES Aug–Sep, 2000–2006	0.24	−7.6	$-44.2/\tau_{0.55}$	N/A	24 h Mean
Sakaeda et al. (2011)	Southern African 30°S–10°N 20°W–50°E	MODIS/CAM/slab ocean model July–October	N/A	−1.6 (land) −2.6 (ocean)	N/A	N/A	24 h Mean
Abel, Highwood, Haywood, and Stringer (2005)	Southern Africa	GCM/AERONET/MODIS	N/A	−3.1 to −3.6	N/A	−14.4 to −17.0	24 h Mean
Yu et al. (2006)	Southeast Asia (Zone 8) 0°N–30°N 90°E–180°E	Terra-MODIS/CERES for ocean Terra-MISR/GOCART for land	0.31 0.13	−6.0 (land) −4.6 (ocean)	$-24.0/\tau_{0.55}$ $-30.7/\tau_{0.55}$	N/A	24 h Mean
This work	Southeast Asia 10°S–20°N 90°E–130°E	Terra-MODIS/CERES/RTM code 2001–2010	0.24 0.17	−5.6 (land) −4.8 (ocean)	$-20.6/\tau_{0.55}$ $-28.5/\tau_{0.55}$	−13.8	24 h Mean
Feng and Christopher (2013)	Southeast Asia 10°S–25°N, 90°E–150°E	Terra-MODIS/CERES Dec. 2006–Nov. 2007	0.27 0.12	−6.4 (land) −5.9 (ocean)	$-20.3/\tau_{0.55}$ $-34.2/\tau_{0.55}$	N/A	24 h Mean

radiative efficiency of $-13\ Wm^{-2}/\tau_{0.55}$ at TOA, which is much lower than the radiative efficiency ($-44\ Wm^{-2}/\tau_{0.55}$) estimated by Patadia et al. (2008) and also lower than the results in our current study. The major reasons are caused by differences between selected time periods. While some studies choose the whole year with both peak and low frequencies of biomass burning; other studies chose data from only high aerosol concentration days. Hence, the differences in the representations of regional aerosols will determine the diurnally averaged radiative efficiency at TOA. Similar differences can be expected in the estimations of radiative efficiency at the surface. Unfortunately, during the last decade, very few studies have calculated ARE_{sfc} or radiative efficiency at the surface, especially over land. The 24-hour mean surface radiative effects of biomass burning aerosols outflow from South Africa were reported to be from $-14.4\ Wm^{-2}$ to $-17.0\ Wm^{-2}$ in Table 2 (Abel et al., 2005), which is in the same range that we report in this study ($-13.8\ Wm^{-2}$). Besides, comparison of our results with previous studies indicates that the estimations of ARE or radiative efficiencies based on satellite or ground-based observations (Feng & Christopher, 2013; Patadia et al., 2008; Yu et al., 2006) are shown to be larger (more negative) than those from model calculations (Abel et al., 2005; Sakaeda et al., 2011; Sena et al., 2013).

4.4. Estimate of vertical profiles of aerosol radiative heating rate

In Fig. 6, we further examined the vertical profiles of shortwave radiative heating rates simulated by the RTM during biomass burning events over Indochina areas observed from an AERONET site on 15th March 2007 (Mukdahan, Thailand, 104.676°E, 16.607°N, purple filled circle in Fig. 6a). This calculation is merely an example from one case day and is not meant to serve as a comprehensive analysis over the region. The smoke event with heavy aerosol loading (AOD at 0.55 μm >0.9) that was prevalent from Cambodia and Vietnam to Thailand in Fig. 6a was due to the occurrence of hundreds of bush and forest fires, burning off crop residue for agricultural activities, and for clearing old pasture in preparation for new spring growth. The height of smoke layers above the ground site is determined based on the nearest CALIPSO overpass, which can also be seen in Fig. 6a (mean height is 2.0 km in this case). In Fig. 6b, the wavelength dependent aerosol properties are derived from AERONET observations (filled circles), and interpolated or extrapolated into RTM wavelengths (open circles) based on empirical equations from previous studies (Reid et al., 2005; Wang & Christopher, 2006). For this case on March 15th 2007, the biomass burning smoke aerosols above the Mukdahan site show the SSA, g and AOD at 0.55 μm as 0.91, 0.67, and 1.41, respectively (Fig. 6b). The surface type for this AERONET site is recognized as crop land based on MODIS 1 km land cover product. These inputs are used in RTM calculations to calculate the vertical profiles of radiative heating rate (Fig. 2b). The elevated smoke layer leads to a shortwave radiative heating of the atmosphere of greater than 0.8 K/day over a significant region of the layer from 2 to 6 km in height (Fig. 6c). This shows that strong biomass burning smoke can have a very significant warming effect on the atmosphere due to their absorptive properties. The vertical profiles of heating rate can be determined by several factors, e.g. the aerosol properties, aerosol layer height, cloud conditions, incoming solar radiation (varied with time), and surface albedo changes. It can be seen in Fig. 6c that the heating rate due to biomass burning smoke aerosols can be apparently enhanced due to increases in AOD. Sena et al. (2013) indicated that the impact of biomass burning aerosols on the energy budget is higher over darker regions such as forest-covered areas than croplands or pasture regions. Comparing to the crop land in this case, the higher diurnally averaged ARE over forests is expected to further enhance the radiative heating in the atmosphere layer which can also be identified based the RTM calculations (Not shown here).

By using vertical profiles of aerosols observed from CALIPSO and spatial distribution of AOD from NOAA-18-AVHRR, Thampi et al. (2009) indicated that the elevated smoke aerosols layers are between 0.6 and 1.6 km over Singapore, which produce an estimated mean atmospheric aerosol heating rate to be ~1.2°K/day. Kedia, Ramachandran, Kumar, and Sarin (2010) observed a similar trend of shortwave aerosol radiative heating over Bay of Bengal and Arabian Sea due to water-soluble aerosols, sea salt, mineral dust, and less than 2% black carbon aerosols (fraction of mass). The higher averaged SSA (0.93) caused by the different optical (AODs), physical (size), and chemical (composition) characteristics of aerosols indicates the dominance of scattering aerosols over the two oceanic regions resulting in a relative lower average atmospheric heating rate over these area of studies than in our work (0.3°K/day and 0.15°K/day over Bay of Bengal and Arabian Sea, respectively). This has also been stated in previous studies that the sensitivity of the direct radiative effect to the aerosol optical properties is primarily driven by differences in SSA, and hence the extent of absorption of short-wave radiation by the atmospheric aerosols (Abel et al., 2005).

5. Summary and conclusions

In this study we have assessed the regional shortwave radiative energy budget under cloud-free conditions from 2001 to 2010, at both the

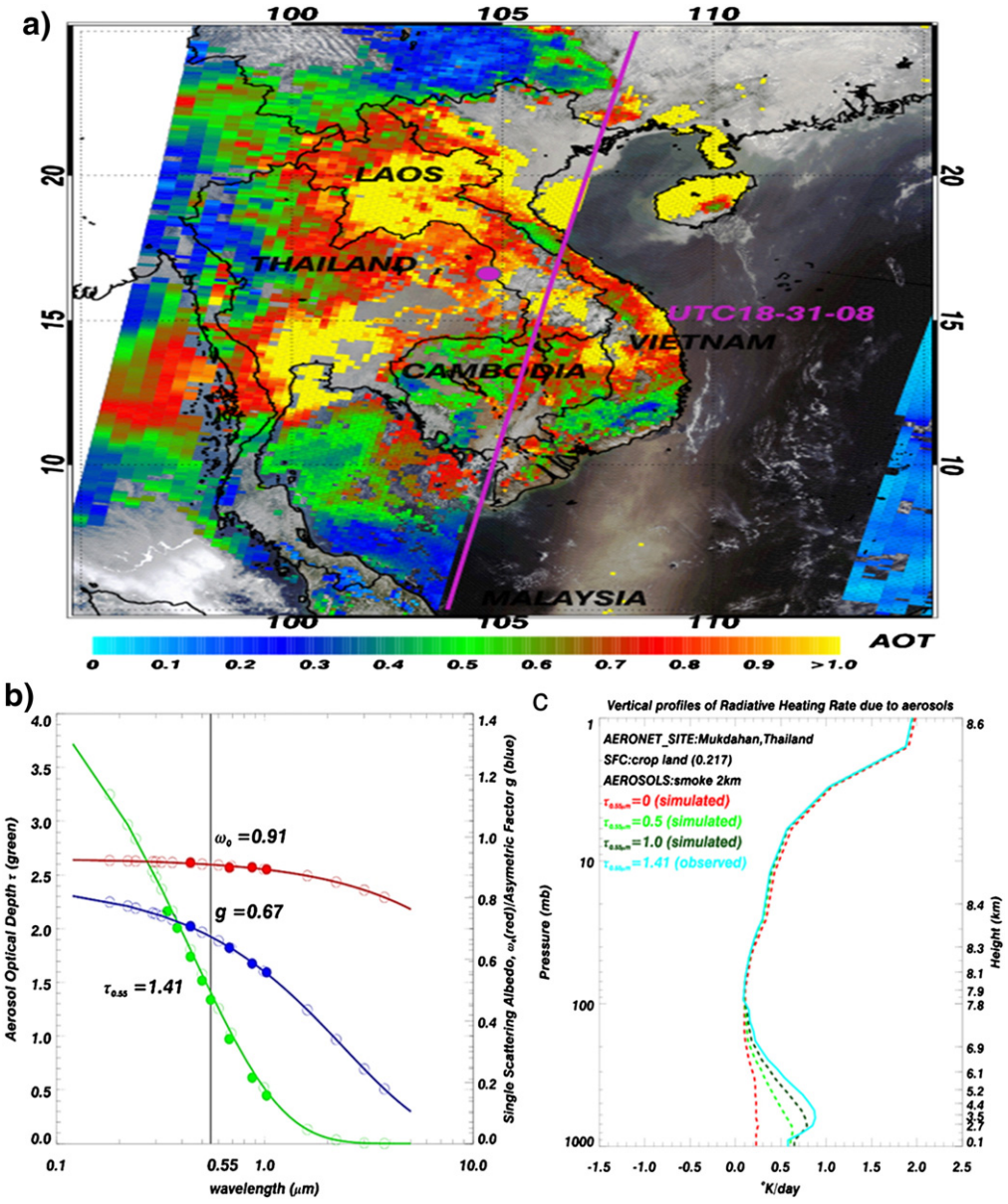

Fig. 6. a) MODIS level 1B radiances from Terra satellite on Mar. 15th, 2007, overlay with MODIS level 2 aerosol optical depth (AOD) at 0.55 μm, where the purple line represents the CALIPSO transect (for aerosol layer height detection). b) Wavelength-dependent aerosol optical depth (green), single scattering albedo (red), and asymmetric factor (blue). Filled circles are observations from AERONET, while these data have been linear fitted to calculate the parameters at wavelengths in the RTM (unfilled circles). The numbers labeled in the figures are the values of these parameters at 0.55 μm. c) Shortwave aerosol radiative heating rates in units of °K/day simulated by the delta four stream RTM during biomass burning events observed from a AERONET site (Mukdahan, Thailand, Feb. 3, 2007). The dash lines in the figure represent heating rate due to aerosols with simulated $\tau_{0.55} = 0$ (red), 0.5 (green), and 1.0 (dark green), respectively. Light blue solid line with ($\tau_{0.55} = 1.41$) is based on real case AOD observations.

TOA and the surface over South East Asia. Spatial and temporal variations of annual ARE are mainly estimated based on satellite (MODIS and CERES) and ground-based measurements (AERONET) supplemented by radiative transfer simulations.

Key findings are as follows:

- The *annual* diurnally averaged TOA shortwave Aerosol Radiative Effect (ARE) in the area of study is -5.6 ± 0.8 Wm^{-2} over land and -4.8 ± 0.7 Wm^{-2} over ocean corresponding to a mean clear-sky midvisible columnar AOD of 0.24 and 0.17, respectively.
- Peak values of ARE_{toa} are during 2004 with values of -7.03 Wm^{-2} over land and -6.14 Wm^{-2} over ocean while the lowest values are in 2008 for land and 2010 for ocean areas.
- By comparing the monthly variation of regional ARE_{toa} with biomass burning emissions from satellite-based datasets, it can be summarized that the regional ARE is impacted not only by the fluxes of smoke aerosols but also by dust, hazes, or industrial emissions, along with other factors such as land use changes and inter-annual climatic variability of the region.
- The spatial distribution analysis of ARE_{toa} shows large geographical variability with significant aerosol impacts over the coastal regions especially in the northern part of SEAS. The diurnally averaged ARE_{toa} is higher in regions with heavy aerosol loadings (e.g. larger AODs), which can locally be even larger than the radiative forcing due to greenhouse gases in some specific regions over SE Asia.
- Comparison of our results with previous studies indicates that the estimations of ARE or radiative efficiencies based on satellite or ground-based observations are shown to be larger (more negative) than those from model calculations.

- The vertical profiles of shortwave radiative heating rates due to biomass burning smoke aerosols show that elevated smoke layers lead to a shortwave radiative heating of the atmosphere of greater than 0.8 K/day.

While the Southeast Asian region has annual cloud cover greater than 60%, the aerosols that are present in cloud-free regions exert a tremendous influence on the radiative energy budget of the earth-atmosphere system. A combination of in situ and satellite measurements coupled with numerical modeling simulations continues to be important for studying the impact of aerosols on climate.

Acknowledgments

This work is supported by NASA Headquarters under the NASA Earth and Space Science Fellowship Program — grant NNX13AN55H. This research is also supported by NASA's radiation sciences program. The satellite data were obtained through the NASA Langley and Goddard Distributed Active Archive Systems. We thank the principal investigators and associated staffs for establishing and maintaining the AERONET sites over SEA used in this investigation. We also thank the anonymous reviewers for their careful reading of our manuscript and their many insightful comments and suggestions.

References

Abel, S. J., Highwood, E. J., Haywood, J. M., & Stringer, M.A. (2005). The direct radiative effect of biomass burning aerosols over southern Africa. *Atmospheric Chemistry and Physics*, *5*, 1999–2018. http://dx.doi.org/10.5194/acp-5-1999-2005.

Begum, B. A., Biswas, S. K., & Hopke, P. K. (2006). Temporal variations and spatial distribution of ambient PM2.2 and PM10 concentrations in Dhaka. *Bangladesh Science of the Total Environment*, *358*, 36–45.

Charlock, T. P., & Alberta, T. L. (1996). The CERES/ARM/GEWEX Experiment (CAGEX) for the retrieval of radiative fluxes with satellite data. *Bulletin of the American Meteorological Society*, *77*, 2673–2683. http://dx.doi.org/10.1175/1520-0477(1996)077<2673:TCEFTR>2.0.CO;2.

Chou, M. -D., Chan, P. -K., & Wang, M. (2002). Aerosol radiative forcing derived from SeaWiFS-retrieved aerosol optical properties. *Journal of the Atmospheric Sciences*, *59*, 748–757. http://dx.doi.org/10.1175/1520-0469(2002)059<0748:ARFDFS>2.0.CO;2.

Christopher, S. A. (2011). Satellite remote sensing methods for estimating clear sky shortwave top of atmosphere fluxes used for aerosol studies over the global oceans. *Remote Sensing of Environment*, *115*, 3002–3006. http://dx.doi.org/10.1016/j.rse.2011.06.003.

Christopher, S. A., Gupta, P., Haywood, J., & Greed, G. (2008). Aerosol optical thicknesses over North Africa: 1. Development of a product for model validation using ozone monitoring instrument, multiangle imaging spectroradiometer, and aerosol robotic network. *Journal of Geophysical Research*, *113*, D00C04. http://dx.doi.org/10.1029/2007jd009446.

Christopher, S. A., & Jones, T. A. (2008). Dust radiative effects over global oceans. *Geoscience and Remote Sensing Letters, IEEE*, *5*, 74–77.

Christopher, S. A., Li, X., Welch, R. M., Reid, J. S., Hobbs, P. V., Eck, T. F., et al. (2000). Estimation of surface and top-of-atmosphere shortwave irradiance in biomass-burning regions during SCAR-B. *Journal of Applied Meteorology*, *39*, 1742–1753. http://dx.doi.org/10.1175/1520-0450-39.10.1742.

Christopher, S. A., Wang, J., Ji, Q., & Tsay, S. -C. (2003). Estimation of diurnal shortwave dust aerosol radiative forcing during PRIDE. *Journal of Geophysical Research*, *108*, 8596. http://dx.doi.org/10.1029/2002jd002787.

Christopher, S. A., & Zhang, J. (2002a). Shortwave aerosol radiative forcing from MODIS and CERES observations over the oceans. *Geophysical Research Letters*, *29*, 1859. http://dx.doi.org/10.1029/2002GL014803.

Christopher, S. A., & Zhang, J. (2002b). Daytime variation of shortwave direct radiative forcing of biomass burning aerosols from GOES 8 imager. *Journal of the Atmospheric Sciences*, *59*(2), 681–691.

Christopher, S. A., Zhang, J., Kaufman, Y. J., & Remer, L. A. (2006). Satellite-based assessment of top of atmosphere anthropogenic aerosol radiative forcing over cloud-free oceans. *Geophysical Research Letters*, *33*, L15816. http://dx.doi.org/10.1029/2005gl025535.

Collins, W. D., Rasch, P. J., Eaton, B. E., Fillmore, D. W., Kiehl, J. T., Beck, C. T., et al. (2002). Simulation of aerosol distributions and radiative forcing for INDOEX: Regional climate impacts. *Journal of Geophysical Research*, *107*, 8028. http://dx.doi.org/10.1029/2000jd000032.

D'Almeida, G. A., Koepke, P., & Shettle, E. P. (1991). *Atmospheric aerosols: Global climatology and radiative characteristics*. A. Deepak Pub (561 pp.).

Davison, P.S., Roberts, D. L., Arnold, R. T., & Colvile, R. N. (2004). Estimating the direct radiative forcing due to haze from the 1997 forest fires in Indonesia. *Journal of Geophysical Research, [Atmospheres]*, *109*, D10207. http://dx.doi.org/10.1029/2003JD004264.

Diner, D. J., Beckert, J. C., Reilly, T. H., Bruegge, C. J., Conel, J. E., Kahn, R. A., Martonchik, J. V., Ackerman, T. P., Davies, R., Ger-stl, S. A. W., Gordon, H. R., Muller, J. P., Myneni, R. B., Sellers, P. J., Pinty, B., & Verstraete, M. M. (1998). Multi-angle Imaging SpectroRadiometer (MISR) – Instrument description and experiment overview. *IEEE T. Geosci. Remote*, *36*, 1072–1087.

Doherty, S. J., Quinn, P. K., Jefferson, A., Carrico, C. M., Anderson, T. L., & Hegg, D. (2005). A comparison and summary of aerosol optical properties as observed in situ from aircraft, ship, and land during ACE-Asia. *Journal of Geophysical Research, [Atmosphere]*, *110*, D04201. http://dx.doi.org/10.1029/2004JD004964.

Eck, T. F., Holben, B. N., Slutsker, I., & Setzer, A. (1988). Measurements of irradiance attenuation and estimation of aerosol single scattering albedo for biomass burning aerosols in Amazonia. *Journal of Geophysical Research, [Atmospheres]*, *103*, 31865–31878. http://dx.doi.org/10.1029/98JD00399.

Feng, N., & Christopher, S. A. (2013). Satellite and surface-based remote sensing of Southeast Asian aerosols and their radiative effects. *Atmospheric Research*, *122*, 544–554. http://dx.doi.org/10.1016/j.atmosres.2012.02.018.

Fu, Q., & Liou, K. N. (1993). Parameterization of the radiative properties of cirrus clouds. *Journal of the Atmospheric Sciences*, *50*, 2008–2025. http://dx.doi.org/10.1175/1520-0469(1993) 050<2008:POTRPO>2.0.CO;2.

Holben, B. N., Tanré, D., Smirnov, A., Eck, T. F., Slutsker, I., Abuhassan, N., et al. (2001). An emerging ground-based aerosol climatology: Aerosol optical depth from AERONET. *Journal of Geophysical Research, [Atmospheres]*, *106*, 12067–12097. http://dx.doi.org/10.1029/2001JD900014.

IPCC (Intergovernmental Panel on Climate Change) (2007). Impacts, adaptation, and vulnerability. In M. L. Parry, O. F. Canziani, J. P. Palutiof, P. J. van der Linden, & C. E. Hanson (Eds.), United Kingdom: Cambridge University Press.

Kahn, R. A., Gaitley, B. J., Martonchik, J. V., Diner, D. J., Crean, K. A., & Holben, B. N. (2005). Multiangle Imaging Spectroradiometer (MISR) global aerosol optical depth validation based on 2 years of coincident Aerosol Robotic Network (AERONET) observations. *Journal of Geophysical Research, [Atmospheres]*, *110*, D10S04. http://dx.doi.org/10.1029/2004JD004706.

Kahn, R. A. (2012). Reducing the uncertainties in direct aerosol radiative forcing. *Surveys in Geophysics*, *33*, 701–721. http://dx.doi.org/10.1007/s10712-011-9153-z.

Kaufman, Y. J., Karnieli, A., & Tanre, D. (2000). Detection of dust over deserts using satellite data in the solar wavelengths. *IEEE Transactions on Geoscience and Remote Sensing*, *38*, 525–531. http://dx.doi.org/10.1109/36.823947.

Kaufman, Y. J., Tanre, D., & Boucher, O. (2002). A satellite view of aerosols in the climate system. *Nature*, *419*, 215–223. http://dx.doi.org/10.1038/nature01091.

Kedia, S., Ramachandran, S., Kumar, A., & Sarin, M. M. (2010). Spatiotemporal gradients in aerosol radiative forcing and heating rate over Bay of Bengal and Arabian Sea derived on the basis of optical, physical, and chemical properties. *Journal of Geophysical Research, [Atmospheres]*, *115*, D07205. http://dx.doi.org/10.1029/2009JD013136.

Lawrence, M. G., & Lelieveld, J. (2010). Atmospheric pollutant outflow from southern Asia: A review. *Atmospheric Chemistry and Physics*, *10*, 11017–11096.

Levy, R. C., Remer, L. A., Mattoo, S., Vermote, E. F., & Kaufman, Y. J. (2007). Second-generation operational algorithm: Retrieval of aerosol properties over land from inversion of Moderate Resolution Imaging Spectroradiometer spectral reflectance. *Journal of Geophysical Research-Atmospheres*, *112*(D13).

Liang, Q., Jaegle, L., Hudman, R. C., Turquety, S., Jacob, D. J., Avery, M.A., et al. (2007). Summertime influence of Asian pollution in the free troposphere over North America. *Journal of Geophysical Research-Atmospheres*, *112*(D12).

Liao, H., & Seinfeld, J. H. (1998). Radiative forcing by mineral dust aerosols: Sensitivity to key variables. *Journal of Geophysical Research*, *103*, 31637–31645. http://dx.doi.org/10.1029/1998jd200036.

Liou, K. -N., Fu, Q., & Ackerman, T. P. (1988). A simple formulation of the delta-four-stream approximation for radiative transfer parameterizations. *Journal of the Atmospheric Sciences*, *45*, 1940–1948. http://dx.doi.org/10.1175/1520-0469(1988)045<1940:ASFOTD>2.0.CO;2.

Liu, H. Y., Jacob, D. J., Bey, I., Yantosca, R. M., Duncan, B. N., & Sachse, G. W. (2003). Transport pathways for Asian pollution outflow over the Pacific: Interannual and seasonal variations. *Journal of Geophysical Research-Atmospheres*(108).

Loeb, N. G., & Kato, S. (2002). Top-of-atmosphere direct radiative effect of aerosols over the tropical oceans from the Clouds and the Earth's Radiant Energy System (CERES) satellite instrument. *Journal of Climate*, *15*, 1474–1484. http://dx.doi.org/10.1175/1520-0442(2002)015<1474:TOADRE>2.0.CO;2.

McClatchey, R. A., Fenn, R. W., Selby, J. E. A., Volz, F. E., & Garing, J. S. (1971). *Optical properties of the atmosphere. Environ. Res. Pap.*, *354*, Bedford, Mass: Air Force Cambridge Res. Lab.

Patadia, F., Christopher, S. A., & Zhang, J. (2011). Development of empirical angular distribution models for smoke aerosols: Methods. *Journal of Geophysical Research D: Atmospheres*, *116*, D14203. http://dx.doi.org/10.1029/2010jd015033.

Patadia, F., Gupta, P., Christopher, S. A., & Reid, J. S. (2008). A Multisensor satellite-based assessment of biomass burning aerosol radiative impact over Amazonia. *Journal of Geophysical Research*, *113*, D12214. http://dx.doi.org/10.1029/2007jd009486.

Podgorny, I. A., Li, F., & Ramanathan, V. (2003). Large aerosol radiative forcing due to the 1997 Indonesian forest fire. *Geophysical Research Letters*, *30*, 1028. http://dx.doi.org/10.1029/2002GL015979.

Procopio, A. S., Artaxo, P., Kaufman, Y. J., Remer, L. A., Schafer, J. S., & Holben, B. N. (2004). Multiyear analysis of Amazonian biomass burning smoke radiative forcing of climate. *Geophysical Research Letters*, *31*, L03108. http://dx.doi.org/10.1029/2003GL018646.

Rajeev, K., Parameswaran, K., Nair, S. K., & Meenu, S. (2008). Observational evidence for the radiative impact of Indonesian smoke in modulating the sea surface temperature of the equatorial Indian Ocean. *Journal of Geophysical Research, [Atmospheres]*, *113*, D17201. http://dx.doi.org/10.1029/2007JD009611.

Reid, J. S., Eck, T. F., Christopher, S. A., Koppmann, R., Dubovik, O., Eleuterio, D. P., et al. (2005). A review of biomass burning emissions part III: Intensive optical properties of biomass burning particles. *Atmospheric Chemistry and Physics*, *5*, 827–849.

Reid, J. S., Hyer, E. J., Johnson, R. S., Holben, B. N., Yokelson, R. J., Zhang, J., et al. (2013). Observing and understanding the Southeast Asian aerosol system by remote sensing: An initial review and analysis for the Seven Southeast Asian Studies (7SEAS) program. *Atmospheric Research*, *122*, 403–468. http://dx.doi.org/10.1016/j.atmosres.2012.06.005.

Reid, J. S., Hyer, E. J., Prins, E. M., Westphal, D. L., Zhang, J. L., Wang, J., et al. (2009). Global monitoring and forecasting of biomass-burning smoke: description of and lessons from the Fire Locating and Modeling of Burning Emissions (FLAMBE) Program. *IEEE Journal of Selected Topics in Applied Earth Observations and Remote Sensing*, *2*, 144–162. http://dx.doi.org/10.1109/jstars.2009.2027443.

Remer, L. A., & Kaufman, Y. J. (2006). Aerosol direct radiative effect at the top of the atmosphere over cloud free ocean derived from four years of MODIS data. *Atmospheric Chemistry and Physics*, *6*, 237–253. http://dx.doi.org/10.5194/acp-6-237-2006.

Remer, L. A., Kaufman, Y. J., Tanre, D., Mattoo, S., Chu, D. A., Martins, J. V., et al. (2005). The MODIS aerosol algorithm, products, and validation. *Journal of the Atmospheric Sciences*, *62*(4), 947–973.

Sakaeda, N., Wood, R., & Rasch, P. J. (2011). Direct and semidirect aerosol effects of southern African biomass burning aerosol. *Journal of Geophysical Research, [Atmospheres]*, *116*, D12205. http://dx.doi.org/10.1029/2010JD015540.

Satheesh, S. K., & Ramanathan, V. (2000). Large differences in tropical aerosol forcing at the top of the atmosphere and Earth's surface. *Nature*, *405*, 60–63. http://dx.doi.org/10.1038/35011039.

Schaaf, C. B., Gao, F., Strahler, A. H., Lucht, W., Li, X. W., Tsang, T., et al. (2002). First operational BRDF, albedo nadir reflectance products from MODIS. *Remote Sensing of Environment*, *83*(1–2), 135–148.

See, S. W., Balasubramanian, R., & Wang, W. (2006). A study of the physical, chemical, and optical properties of ambient aerosol particles in Southeast Asia during hazy and nonhazy days. *Journal of Geophysical Research*, *111*, D10S08. http://dx.doi.org/10.1029/2005JD006180.

Sena, E. T., Artaxo, P., & Correia, A. L. (2013). Spatial variability of the direct radiative forcing of biomass burning aerosols and the effects of land use change in Amazonia. *Atmospheric Chemistry and Physics*, *13*, 1261–1275. http://dx.doi.org/10.5194/acp-13-1261-2013.

Smith, G. L. (1994). Effects of time response on the point spread function of a scanning radiometer. *Appl. Opt.*, *33*, 7031–7037.

Smirnov, A., Holben, B., Eck, T., Dubovik, O., & Slutsker, I. (2000). Cloud screening and quality control algorithms for the AERONET database. *Remote Sensing of Environment*, *73*, 337–349. http://dx.doi.org/10.1016/S0034-4257(00)00109-7.

Srivastava, R., Ramachandran, S., Rajesh, T. A., & Kedia, S. (2011). Aerosol radiative forcing deduced from observations and models over an urban location and sensitivity to single scattering albedo. *Atmospheric Environment*, *45*, 6163–6171. http://dx.doi.org/10.1016/j.atmosenv.2011.08.015.

Tegen, I. (2003). Modeling the mineral dust aerosol cycle in the climate system. *Quaternary Science Reviews*, *22*, 1821–1834. http://dx.doi.org/10.1016/S0277-3791(03)00163-X.

Tegen, I., & Lacis, A. A. (1996). Modeling of particle size distribution and its influence on the radiative properties of mineral dust aerosol. *Journal of Geophysical Research*, *101*, 19237–19244. http://dx.doi.org/10.1029/95jd03610.

Thampi, B. V., Rajeev, K., Parameswaran, K., & Mishra, M. K. (2009). Spatial distribution of the Southeast Asian smoke plume over the Indian Ocean and its radiative heating in the atmosphere during the major fire event of 2006. *Geophysical Research Letters*, *36*, L16808. http://dx.doi.org/10.1029/2009GL039316.

Wang, J., & Christopher, S. A. (2006). Mesoscale modeling of Central American smoke transport to the United States: 2. Smoke radiative impact on regional surface energy budget and boundary layer evolution. *Journal of Geophysical Research*, *111*, D14S92. http://dx.doi.org/10.1029/2005JD006720.

Wang, J., Christopher, S. A., Reid, J. S., Maring, H., Savoie, D., Holben, B. N., et al. (2003). GOES 8 retrieval of dust aerosol optical thickness over the Atlantic Ocean during PRIDE. *Journal of Geophysical Research*, *108*, 8595. http://dx.doi.org/10.1029/2002jd002494.

Wang, W., Huang, J., Zhou, T., Bi, J., Lin, L., Chen, Y., et al. (2013). Estimation of radiative effect of a heavy dust storm over northwest China using Fu–Liou model and ground measurements. *Journal of Quantitative Spectroscopy and Radiative Transfer*, *122*, 114–126. http://dx.doi.org/10.1016/j.jqsrt.2012.10.018.

Yu, H., Kaufman, Y. J., Chin, M., Feingold, G., Remer, L. A., Anderson, T. L., et al. (2006). A review of measurement-based assessments of the aerosol direct radiative effect and forcing. *Atmospheric Chemistry and Physics*, *6*, 613–666. http://dx.doi.org/10.5194/acp-6-613-2006.

Zhang, J., Christopher, S. A., Remer, L. A., & Kaufman, Y. J. (2005a). Shortwave aerosol radiative forcing over cloud-free oceans from Terra: 1. Angular models for aerosols. *Journal of Geophysical Research*, *110*, D10S23. http://dx.doi.org/10.1029/2004jd005008.

Zhang, J., Christopher, S. A., Remer, L. A., & Kaufman, Y. J. (2005b). Shortwave aerosol radiative forcing over cloud-free oceans from Terra: 2. Seasonal and global distributions. *Journal of Geophysical Research*, *110*, D10S24. http://dx.doi.org/10.1029/2004jd005009.

Zou, L. Y., & Hooper, M.A. (1997). Size resolved airborne particles and their morphology in central Jakarta. *Atmospheric Environment*, *31*, 1167–1172.